ResearchGate

See discussions, stats, and author profiles for this publication at: https://www.researchgate.net/publication/228376329

Optical Emission and Energy Transfer in Nanoparticle– Nanorod Assemblies: Potential Energy Pump System for Negative Refractive Index Materials

ARTICLE *in* THE JOURNAL OF PHYSICAL CHEMISTRY C · NOVEMBER 2008

Impact Factor: 4.77 · DOI: 10.1021/jp8006238

CITATIONS
22

READS
55

4 AUTHORS, INCLUDING:

Alexander O Govorov
Ohio University
143 PUBLICATIONS **4,614** CITATIONS
SEE PROFILE

Nicholas Kotov
University of Michigan
445 PUBLICATIONS **26,671** CITATIONS
SEE PROFILE

Available from: Nicholas Kotov
Retrieved on: 15 January 2016

THE JOURNAL OF PHYSICAL CHEMISTRY C

Subscriber access provided by KENT STATE UNIV KENT

Article

Optical Emission and Energy Transfer in Nanoparticle#Nanorod Assemblies: Potential Energy Pump System for Negative Refractive Index Materials

Ashish Agarwal, George D. Lilly, Alexander O. Govorov, and Nicholas A. Kotov

J. Phys. Chem. C, **2008**, 112 (47), 18314-18320 • Publication Date (Web): 31 October 2008

Downloaded from http://pubs.acs.org on January 7, 2009

More About This Article

Additional resources and features associated with this article are available within the HTML version:

- Supporting Information
- Access to high resolution figures
- Links to articles and content related to this article
- Copyright permission to reproduce figures and/or text from this article

View the Full Text HTML

ACS Publications
High quality. High impact.

The Journal of Physical Chemistry C is published by the American Chemical Society. 1155 Sixteenth Street N.W., Washington, DC 20036

ARTICLES

Optical Emission and Energy Transfer in Nanoparticle−Nanorod Assemblies: Potential Energy Pump System for Negative Refractive Index Materials

Ashish Agarwal,[†] George D. Lilly,[†] Alexander O. Govorov,*[,‡] and Nicholas A. Kotov*[,†]

Department of Chemical Engineering, University of Michigan, Ann Arbor, Michigan 48109, and Department of Physics and Astronomy, Ohio University, Athens, Ohio 45701

Received: January 22, 2008; Revised Manuscript Received: June 2, 2008

Gold nanorods (NRs) in different arrangements represent the most plausible system for the creation of negative refractive index materials (NIMs) in the optical frequency range. Among other challenges, one of the major limitations of present day NIMs is their large amount of energy dissipation which frustrates the restoration of near field modes. To take advantage of exciton−plasmon interactions, an optical system consisting of semiconductor nanoparticles (NPs) and Au NRs can continuously pump energy into the NIM resonator. Superstructures with promising properties were achieved by assembly of CdTe nanoparticles on the surface of nanorods by using streptavidin−biotin bioconjugation where NP→NR energy transfer occurs with great efficiency. On the initial layer of bioconjugated NPs, the second layer is formed due to nonspecific interactions, which is manifesting in unusual spectral behavior and dependence of lifetime on NP concentration. By varying the ratio of NPs per NR, the amount of energy transfer can be controlled, while the diameter of NPs and wide overlap offers the possibility to tune the wavelength of the pumping light.

Introduction

One of the most fascinating types of metamaterials that is actively researched is negative refractive index materials (NIMs). Early theoretical discussions by Veselago[1] showed that an isotropic media with both negative permittivity, ε, and permeability, μ, will exhibit a negative refractive index along with several other interesting properties. However, such materials remained a curiosity for decades because no naturally occurring materials exhibit simultaneous negative ε and μ over a common frequency range. Recent theoretical demonstration by Pendry[2] showed that an ideal Veselago lens (flat slab in vacuum with $\varepsilon = \mu = -1$) can not only focus light from an object to form an image but can do so with subwavelength resolution ($\Delta x < \lambda$). Such lens has been termed the "perfect lens" and has created a new surge of interest in the development of artificial metamaterials with negative refractive index. NIMs have also been suggested as novel materials for usage in biological and security imaging, biomolecular fingerprinting, remote sensing, cloaking devices, and guidance in zero visibility weather condition.[3−6]

The two most common approaches to fabricate NIMs take advantage of photonic crystals[7−10] or plasmonic periodic metal-dielectric nanostructures.[11−13] NIM photonic crystals are based on the excitation of photonic band gaps with negative slope to support negative phase velocity in the medium and are limited in their performance due to scattering from surface imperfections. In metal-dielectric nanostructures the displacement currents near plasmonic resonances are used to produce both negative permittivity and negative permeability. One-dimensional gold and silver nanostructures in various arrangements have been theoretically and experimentally shown to have negative refractive index.[14,15] Importantly, operating near plasmonic resonances in metallic NIMs makes their response strongly dispersive and lossy;[16] thus, restraining the restoration of near field modes which are required for sub wavelength resolution in the image.

One way to reduce losses in metallic systems is to operate away from the resonances,[17] however this would weaken the diamagnetic response of the medium potentially causing it to no longer have the effective negative permeability. The other way is to compensate the losses by providing a gain medium. The conventional way of adding a gain medium is by sandwiching a 2D layer between the NIM, but this requires an impedance match at the interface to avoid losses by reflection.[18,19] Submerging entire metallic nanoparticles (NPs) in dye molecules which act as a gain medium has also been suggested.[20] Dyes, however, have limited lifetime and bleach rapidly. As well, there are inherent optical limitations related to Stocks shift in organic dyes that limit their applicability to NIMs.

In this paper, we demonstrate that semiconductor NPs assembled with metallic nanorods or similar optical media can be used as a potential gain material for NIMs. Both experiments and corresponding theoretical calculations describing coupled optical oscillators in semiconductor (exciton) and metal (plasmon) clearly indicate that the excitonic energy of NPs can be funneled into the plasmon of gold nanorods (NRs). The actual manufacturing of such assemblies was accomplished using fairly universal the biotin−streptavidin (B-SA) bioconjugation strategy between CdTe NPs and Au NRs. Strong quenching of CdTe NPs, which indicates energy transfer into Au NRs was observed.

* To whom correspondence should be addressed. E-mail: govorov@ohiou.edu (A.O.G.); kotov@umich.edu (N.A.K.).
[†] Ohio University.
[‡] University of Michigan.

10.1021/jp8006238 CCC: $40.75 © 2008 American Chemical Society
Published on Web 10/31/2008

Given sufficient intensity and coherence of the excitation of NPs away from the resonance band of NRs, the energy transfer can compensate for losses in NIMs.

Experimental Section

Materials. Hexadecyltrimethylammonium bromide (CTAB), silver nitrate, ascorbic acid, sodium borohydride, gold(III) chloride, L-cystine, thioglycolic acid (TGA) were purchased from Aldrich and used without further purification. Deionized water (Barnstead, E-pure system) with 18 MΩ was used in preparation of solutions. Streptavidin (SA) and *D*-biotin (B) were obtained from Aldrich. 1-Ethyl-3-(3-dimethylamino propyl) carbodiimide hydrochloride (EDC) and *N*-hydroxy-sulfosuccinimide (NHS) were purchased from Aldrich and Merck for bioconjugation, respectively.

Synthesis. Au NRs of average aspect ratio 3.7 (length 48 ± 5 nm and width 13 ± 2 nm) were synthesized by a method described elsewhere.[21,22] Synthesized NRs were purified by removing excess salts and stabilizer using centrifugation and redispersion into deionized water. The Au NRs are dispersed in deionized water to achieve a concentration of 10^{-8} M of NRs in the solution. CdTe NPs were synthesized with L-cystine stabilizer (average diameter 3 nm) for bioconjugated assembly as reported previously.[23] The particles were used as synthesized (average concentration 10^{-5} M of NPs) without any further purification. Binding of biotin to L-cystine NPs is performed as described in literature.[24,25]

Bioconjugation of Au NRs. A layer of poly(acrylic acid) (PAA) is adsorbed onto the surface of NRs by adding 1.5 mL of 10 mg/mL PAA solution to 1 mL of the stock gold NR solution. The mixture is stirred for 3 h followed by two cycles of centrifugation and redispersion to remove excess PAA in the solution.[26] The layer of PAA provides the −COOH functional group required for the conjugation. The PAA coated nanorods are dispersed in 1 mL of PBS 6.0 buffer solution followed by the addition of 100 μL of 0.2 M EDC and 100 μL of 0.2 M NHS. After 20 min, the reaction mixture is added with 20 μL of SA. The EDC/NHS mixture forms an active ester intermediate with the gold nanorods which undergoes amidation reaction with the $-NH_2$ group in SA to yield the conjugate. The reaction mixture is stored in refrigerator at 4 °C overnight following centrifugation and redispersion in buffer to remove the unconjugated SA.

Instrumentation. Photoluminescence spectrums were recorded using Fluoromax-3 spectrofluorometer (Jobin Yvon/SPEX Horiba, NJ). UV−visible absorption spectra were recorded using Agilent (former HP) UV−vis spectrophotometer.

Results

We used two approaches for the preparation of NR−NP complexes: electrostatic and bioconjugation. In the electrostatic method of assembly we used positively charged NRs and negatively charged NPs bearing thioglycolic acid as a stabilizer. Electrostatically bound structures were appealing to us because they can potentially reduce the gap between the nanoscale building blocks, and thus, increase the resonance amplitude in exciton-plasmon hybrid states. However, NP−NR superstructures assembled electrostatically displayed approximately an order of magnitude lower efficiency of NP→NR energy transfer than protein-bound systems potentially due to the dynamic nature of the electrostatic assemblies where NPs migrate in and out of the range of plasmon-exciton interactions with NRs. Thus, all the data presented here refer to the system with B-SA linker.

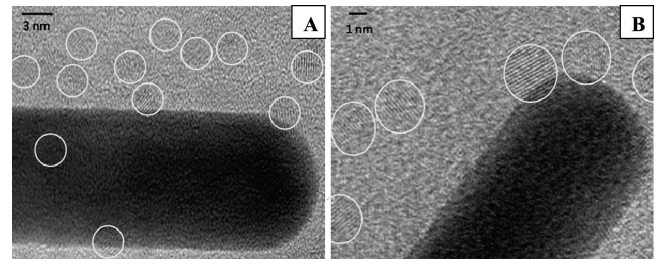

Figure 1. (A) TEM image of bioconjugated assembly, ratio of NPs/NR = 25. (B) HRTEM image showing the lattice structure of NP bioconjugated to NR.

TABLE 1: Lifetime Values and Electrokinetic (ζ) Potentials for Bioconjugated Assembly at Various NP/NR Ratios[a]

	bioconjugated assembly	
NP/NR ratio	lifetime (ns)	ζ potential (mV)
∞	26.66	−31.1
1000	13.00	−0.90
500	7.07	6.60
333	4.33	4.70
250	3.00	5.20
125	2.00	4.10
50	0.62 (extrapolated value)	5.40
25	0.31 (extrapolated value)	5.30
0	NA	30.60

[a] Extrapolated values were obtained from Stern−Volmer fit, eq S1 in Supporting Information.

Structure of the NP−NR Complexes. Bioconjugates of NPs and other nanocolloids bearing biological groups with strong mutual affinity allow one to create sophisticated NP assemblies.[27−29,31,33] As such, due to specific binding between SA and B, mixing of NR-SA and NP-B leads to superstructures with NPs attached to the surface of NRs (Figure 1A). The same conclusion can be reached from the study of electrokinetic (ζ) potentials of the nanocolloids (Table 1). As the ratio of the number of CdTe NPs per Au NR (i.e., NP/NR ratio) increases, the zeta potential gradually changes from positive to negative. The change of sign of zeta potential is reflective of the increase of the density of NPs attached to NRs.

The separation between the NP and NR in bioconjugated structures is due to the presence of bilayers of CTAB, streptavidin−biotin and L-cystine. Assuming the simple case of attachment via SA-B connection, the distance between the center of the NPs and the surface of the NR is estimated to be Δ_{BA} = 6.5 nm. Distances between the two components are established from TEM images at higher magnification to give an average NP−NR distance of 5 nm which coincides with the estimates above quite well. In case of formation of additional shells of NPs attracted by, for instance, strong van der Waals forces to the initial coating of NPs, the distance between the NR surface will increase by a few more nanometers depending on the NP layer geometry. The signs of NP clustering around NRs beyond a simple monolayer can be seen in Figure 1A. This process can be treated as if the self-assembly of the first layer catalyzes the adherence of the NP in the second layer. At the same time it is self-limited due to strong repulsion of similarly charged NPs in the shells. The same processes are observed during the layer-by-layer assembly of NPs.

One also needs to remember that the NP−NR bioconjugates are 3D structures, which creates difficulties in traditional TEM imaging. Bringing both components of the assemblies, NPs and NRs, in focus at the same time, becomes more difficult than for much simpler 2D arrangements of NRs or NPs separately.

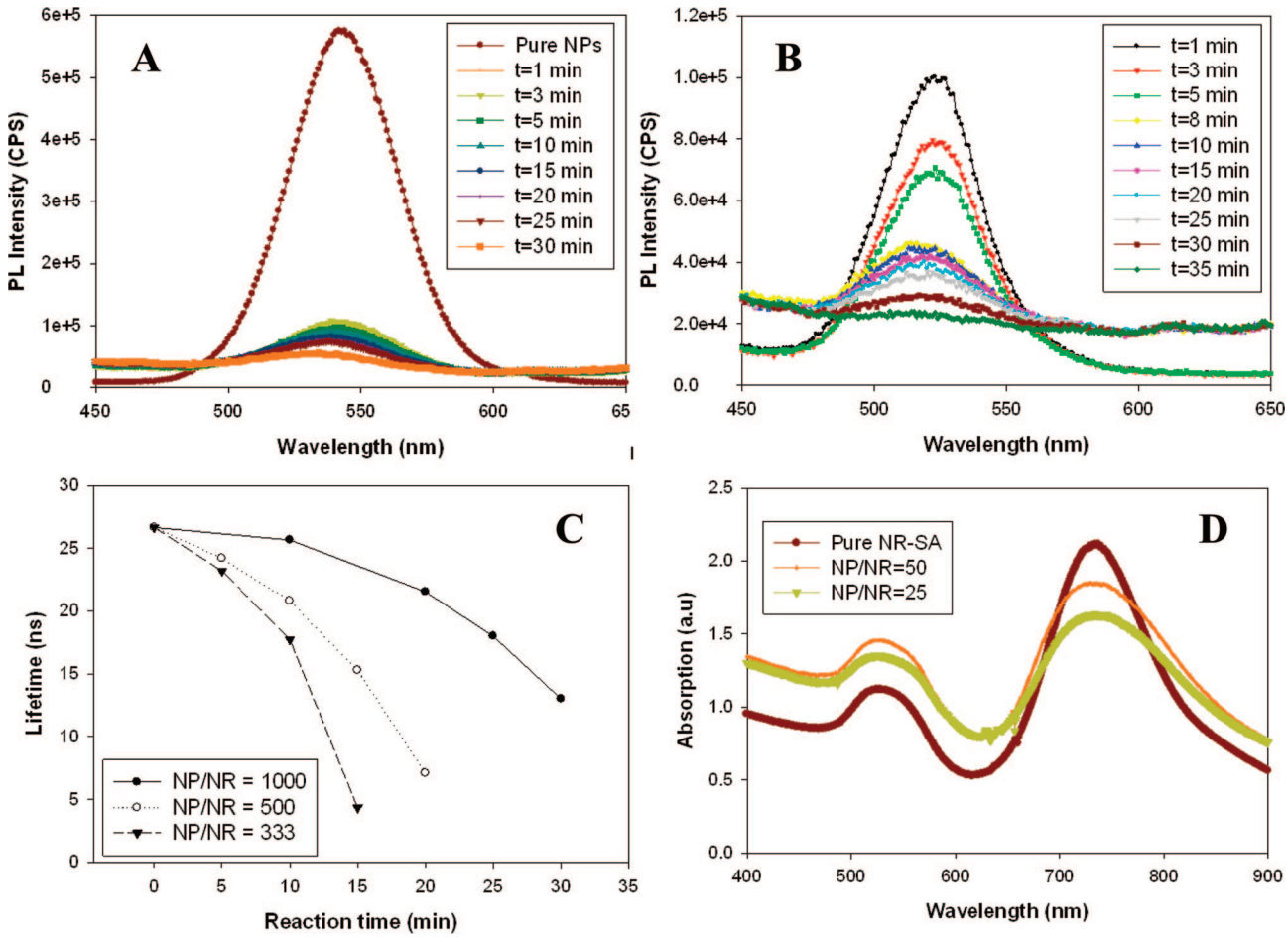

Figure 2. (A) Consecutive fluorescent spectra for the formation of NP−NR bioconjugated assembly with NP/NR = 125. (B) Consecutive fluorescent spectra for the formation of NP−NR bioconjugated assembly with NP/NR = 12.5. (C) Change of lifetime values of NPs during the period of formation of bioconjugated NP−NR assembly. (D) UV−vis of NR-SA before and after assembly with NP-B. Excitation wavelength 350 nm.

However, we were able to do it when both building blocks are properly positioned. In Figure 1B one can clearly distinguish the lattice planes corresponding to CdTe particles and Au NR. The CdTe NPs show a lattice spacing of 0.249 nm which corresponds to the (111) plane of CdTe nanocrystal with a literature value of lattice spacing of 0.229 nm.[30] The distribution of the NPs along the length of the rod is fairly random; no preference is given to the ends of the rods or their sides (Figure 1). We also see evidence (Figure 1A) of NP clustering around the NRs and formation of double shells. The primary bond between the first layer of NPs and NRs is of SA-B nature, while subsequently the particles in the secondary shell are attached by nonspecific interactions.

Optical Properties. Based on previous studies,[27−29,31−33] NP−NR distances observed in Figure 1 are expected to result in strong interactions between exciton and plasmon states in the semiconductor and metallic particles, respectively. This interaction can result in both luminescence enhancement[34,35] as well as quenching.[32,36] NP superstructures studied previously included the assemblies of CdTe NWs and Au NPs.[37] The general geometrical configuration of the superstructure in the present case is similar to those reported before[25,29,33,37] with the exception that the symmetries CdTe and Au components are switched, i.e. the axial rodlike structures here are made from metal as opposed to the semiconductor wires in the previous publication. This results in radical differences in optical behavior of the superstructures. In the present case, when the rods are made from gold, we observe very strong quenching of CdTe excitons that are attributed to energy transfer from NP to Au NRs via a resonance state (Figure 2A−C), as opposed to the enhancement of exciton emission due to coupled field stimulation from Au NPs observed previously.

The quenching of NP luminescence in bioconjugated superstructures progresses over a period of 30 min, following the typical B-SA binding kinetics.[33,38,39] Upon addition of NP-B into a solution containing NR-SA we find that initially there is a fast drop in PL intensity within first 3 min, followed by much slower gradual decrease over the next 27 min. The early stages of the kinetic curve should cover mostly the formation of B-SA links, while the later stages should mostly describe attachment via nonspecific interactions. At the moment these two parts are difficult to separate. However, more detailed investigation of this process will make it possible when such data might be necessary. Note there is an increase of the background signal in the "wings" of the luminescence peak for the later stages of assembly, which is attributed to stronger scattering of the assembled structures. When one compares quenching data from the two systems with NP/NR ratios different by 10 times (Figure 2A,B), the kinetics becomes about 10 times slower in accordance with general theory of reaction rates $\partial[\mathrm{NP-NR}]/\partial t = k[\mathrm{NP}][\mathrm{NR}]$, giving the degree of quenching over a period of ca. 30 min for NP/NR = 12.5 approximately equal to that observed for 3 min for NP/NR = 125. Importantly, for both NP/NR ratios the final state is almost complete quenching of NP luminescence (Figure 2A,B).

The CdTe fluorescence peak spanning 480 to 580 nm overlaps with the transverse plasmon resonance (480−550 nm) of the NR. The coupling of excitons from NP with plasmons is believed to be able to funnel energy into the NR.[43] NPs are excited
in the near UV wavelengths and would interact minimally with the incident light (optical wavelengths) and avoid any undesirable effects on the effective properties of the material at optical wavelengths. The presence of CdTe NPs around NR, however, slightly dampen and broaden the plasmonic response of the NRs (Figure 2D), which may or may not be significant for actual NIM structures. Slight broadening of the plasmon resonance may actually be advantageous for NIMs as it provides a broader wavelength range over which the NIM response could be realized. The broadening of the plasmon peak and the presence of semiconductor NPs at the interface may actually serve as a convenient control parameter to vary the degree of resonance/off-resonance excitation for NIM structures.

The conjugated NPs remain stable in solution and show same plasmon absorption as in Figure 2D for 7 days. The plasmonic absorption starts decreasing after 7 days and the solution shows aggregated particles after 12 days which may be caused due to protein denaturation. Since the NP−NR assembly is robust one can use these structures by depositing them onto substrates or thin films. The stability period is also sufficient to carry out any polymerization reaction necessary to permanently fix the assemblies.

The effect of superstructure formation on the lifetime of CdTe excitons was also measured (Table 1 and Figure 2C). For small NP/NR ratios this is fairly difficult to do due to low overall luminescence and strong quenching, but for ratios in the range of 333−1000 the lifetime, τ, can be measured during the assembly process. As expected, formation of the NP−NR superstructure results in significant decrease of the emission lifetime because of the NP→NR energy transfer processes. Larger NP/NR ratios results in slower kinetics which indicates the change in general kinetic description of the process for high concentrations of NPs and potential saturation processes when the amount of NPs is sufficient to occupy all available surfaces on NRs. Simple geometrical calculations for closely packed structure of CdTe NPs on Au NRs with the dimensions used here correspond to 70 NPs per one NR, however, apparently greater number of NPs may cluster around the NRs in 2 or more shells due to the nonspecific clustering of NPs.

We observed complete quenching as NP/NR ratio reached 25. So, we were unable to experimentally measure the lifetime of the assembly at this ratio because of the low luminescence intensity. This lifetime value was estimated by extrapolating the Stern−Volmer quenching kinetics (Supporting Information). It was found to be 0.314 ns. The lifetime data are shown in Table 1, the data in Figure 2C, and the quantum yield for the NPs equal to $Y = 0.115$ were used as input parameters in the theoretical calculations described below as well as in the ensuing discussion.

Blue Shift of Emission Peak. Interestingly, we observe a noticeable blue shift in the emission spectra of NPs by ∼5 nm as formation of the bioconjugated assembly proceeds (Figure 2A,B and Figure 3). This shift may come from the reduction of Coulomb binding energy, E_{Coulomb}, of an exciton in CdTe NPs due to an enhanced dielectric screening in a bioconjugated assembly according to the standard equation of quantum confinement effect in semiconductor NPs:

$$E_{\text{exc}} = E_{\text{bulk}} + h^2/2m^*d^2 - E_{\text{Coulomb}} \quad (1)$$

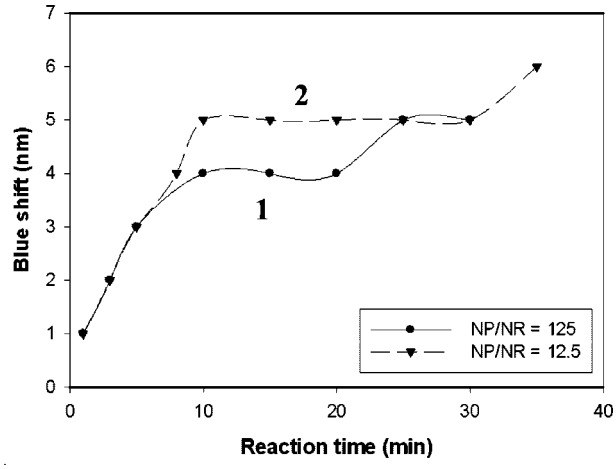

Figure 3. Position of the maximum of emission peak during the period of formation of two bioconjugated assemblies with NR =125 (1) and NR = 12.5 (2).

where E_{exc} is the energy of emitted exciton considered to be equal to band gap energy in the quantum confined state, E_{bulk}, is the band gap in the bulk state, h is Plank constant, m^* is the reduced mass of electron and hole $m^* = 1/m_e + 1/m_h$, d is the diameter of the NP. Upon assembly, the Coulomb interaction between an electron and hole inside CdTe NP becomes slightly lower since the average dielectric constant of the surrounding increases due to the presence of the neighboring metal and semiconductor NPs.

Theoretical Model and Discussion. Quenching of emission and shortening of exciton lifetime in the NP-NR superstructures can be explained using a model based on the exciton-plasmon resonance (Figure 4) taking place when emission peak of excitons in NPs and adsorption peak of the plasmons in NRs display a spectral overlap. In a NP-NR complex, oscillators corresponding to excitons in NPs and plasmons in NRs couple via simple Coulomb forces. Since NP-NR complexes are in liquid, they are randomly oriented with respect to the incident electric field, $\vec{E}_0$ (Figure 4a). To obtain analytical estimates, we will treat NRs as infinite cylinders. In addition, we will consider here the near field regime $\lambda \gg d$, where λ and d is the wavelength of light and NP-NR distance, respectively. Considering the data in Figure 1, this assumption is certainly valid. The electric field in the vicinity of infinite metal cylinder is described by the potential: $\phi = -\vec{E}_0\vec{r} + (\varepsilon_{\text{Au}} - \varepsilon_0)/(\varepsilon_{\text{Au}} + \varepsilon_0)\cdot(a_{NR}^2/4\rho^2)\vec{E}_0\vec{r}$, where a_{NR} is the NR diameter, ρ is the distance to the NR axis, and ε_{Au} and ε_0 are the dielectric constants of metal and matrix, respectively.[40] The light absorption rate in a CdTe NP is proportional to $\langle\vec{E}\cdot\vec{E}^*\rangle_\Omega$, where $\vec{E}$ is the electric field in the vicinity of NR and Ω is the solid angle. Averaging over Ω is introduced to take into account random orientations of NRs with respect to the incident light. After simple algebra, we obtain $\langle\vec{E}\cdot\vec{E}^*\rangle_\Omega = E_0^2[1 + (2/3)\gamma\gamma^*(a_{NR}^4/d^4)]$, where $\gamma = (\varepsilon_{\text{Au}} - \varepsilon_0)/(\varepsilon_{\text{Au}} + \varepsilon_0)$. The intensity of emission from a CdTe NP is derived from the rate equations published previously for molecular systems with fluorescent dyes.[35] Note that molecular and nanoscale superstructures have an important difference. An excitation in molecular systems is described by one exciton with a given direction of dipole moment. A spherical NP has three optically active excitons with optical dipoles along x, y, and z axes. Due to fast spin relaxation at room temperature, we can assume that optical excitation creates almost equal populations of excitons with different orientation in respect to a NP axis. Therefore, to calculate the resultant emission of a NP, we have

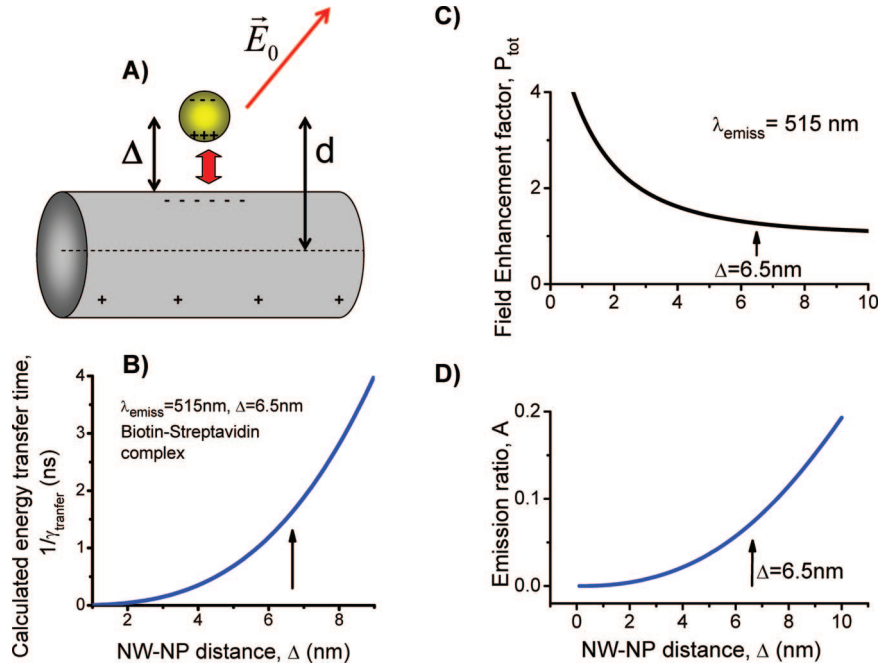

Figure 4. (A) Model of NP−NR system. Red arrow shows the process of energy transfer. (B) Calculated energy rate as a function of NP−NR separation. (C and D) Theoretical results for enhancement factor and emission ration.

to take into account all three orientations of excitons. At room temperature, the emission intensity of NP is given by[27,31]

$$I_{\text{emiss}}(\lambda_1,\lambda_{\text{emiss}}) = \frac{P(\lambda_{\text{emiss}})\cdot\gamma^0_{\text{rad}}\cdot P(\lambda_1)\cdot I^0_{\text{abs}}}{P(\lambda_{\text{emiss}})\cdot\gamma^0_{\text{rad}} + \gamma^0_{\text{non-rad}} + \gamma_{\text{transfer}}(\lambda_{\text{emiss}})} \tag{2}$$

where λ_1 and λ_{emiss} are the wavelengths of exciting light and emitted photons, respectively, $P(\lambda) = \langle\vec{E}\cdot\vec{E}^*\rangle_\Omega/E_0^2$ is the averaged field enhancement factor for a NP in the vicinity of a NR, and I^0_{abs} and γ^0_{rad} are the light absorption and radiative rates of a CdTe NP in the absence of a gold NR. The denominator in eq 2 represents the total recombination rate of an exciton $\gamma_{\text{rec}} = P(\lambda_{\text{emiss}})\cdot\gamma^0_{\text{rad}} + \gamma^0_{\text{non-rad}} + \gamma_{\text{transfer}}(\lambda_{\text{emiss}})$, where $\gamma^0_{\text{non-rad}}$ is the nonradiative recombination rate and $\gamma_{\text{transfer}}(\omega_{\text{emiss}})$ is the rate of NP → NR energy transfer. The parameter $P(\lambda_{\text{emiss}})\cdot\gamma^0_{\text{rad}}$ in eq 2 describes the radiative emission rate of an exciton in a NP in the presence of a NR. Similarly, $P(\lambda_1)\cdot I^0_{\text{abs}}$ is a metal-modified absorption rate of a CdTe NP. In particular, we can see that the factor $P(\lambda)$ is an important parameter of the system. From eq 2, we obtain the ratio between emission intensities before and after conjugation:

$$A(d,\lambda_1,\lambda_{\text{emiss}}) = \frac{I_{\text{emiss,complex}}}{I_{\text{emiss,0}}} = P_{\text{tot}}\frac{\gamma_{\text{rad,av,0}} + \gamma_{\text{non-rad}}}{\gamma_{\text{transfer}} + \gamma_{\text{rad,av,0}}P(\lambda_{\text{emiss}}) + \gamma_{\text{non-rad}}} \tag{3}$$

where $P_{\text{tot}} = P(\lambda_1)P(\lambda_{\text{emiss}})$ is the resultant field enhancement factor for the emission; $\gamma_{\text{non-rad}} = (1-Y)\cdot\gamma^0_{\text{rec}}$ and $\gamma^0_{\text{rad}} = Y\cdot\gamma^0_{\text{rec}}$, where Y is the quantum yield and $\gamma^0_{\text{rec}} = 1/\tau^0_{\text{rec}}$ is the recombination rate of excitons in NPs in the absence of metal NRs. The transfer rate γ_{transfer} describes the process of Förster-like energy transfer NP→NR (Figure 4A). This process comes from the Coulomb interaction between a photoexcited exciton in a CdTe-NP and plasmons in a NR. A convenient formalism to calculate the rate γ_{transfer} is based on the response function and is given in refs 27 and 31.

Here we give a result for small NP−NR distances, $\Delta < a_{NR}$:

$$\gamma_{\text{transfer}} = \frac{(ed_{\text{exc}})^2}{\hbar\varepsilon^2_{\text{eff}}}\frac{\varepsilon_0}{3\Delta^3}\text{Im}\frac{(\varepsilon_m-\varepsilon_0)}{\varepsilon_0+\varepsilon_m} \tag{4}$$

where $\varepsilon_{\text{eff}} = (2\varepsilon 0 + \varepsilon_{NP})/3$ and d_{exc} is the exciton dipole moment and ε_{NP} is the dielectric constant of CdTe. We note that the transfer rate in eq 4 was calculated as an averaged transfer rate of three types of excitons in a CdTe NP: $\gamma_{\text{transfer}} = (\gamma_{\text{tr},x} + \gamma_{\text{tr},y} + \gamma_{\text{tr},z})/3$, where $\gamma_{\text{tr},i}$ is the transfer rate for the exciton with a dipole moment in the i-direction. For small distances ($\Delta < R_{NR}$), $\gamma_{\text{transfer}} \propto 1/\Delta^3$.[41] For large distances ($\Delta > R_{NR}$), eq 4 is no longer applicable and $\gamma_{\text{transfer}} \propto 1/\Delta^5$.[29] Equation 4 was used to obtain estimates for bioconjugated complexes with the following parameters: $a_{NR} = 15$ nm, $R_{NP} \approx 1.5$ nm (CdTe NP radius) and $\Delta = 6.5$ nm (length of SA-B linker length). Exciton emission from our CdTe NPs has the following characteristics: $\tau^0_{\text{rad}} = 26.6$ ns and $Y \approx 0.115$ (see above). The dielectric constant of the metal was taken from the tables[42] and the other dielectric parameters were chosen as $\varepsilon_{NP} = \varepsilon_{\text{CdTe}} = 7.2$ and $\varepsilon_0 = \varepsilon_{\text{water}} = 1.8$. The exciton dipole moment was estimated from the radiative time: $d_{\text{exc}} = 0.53$ Å. Results of calculations are summarized in Figure 4B−D. For the assembly, we obtain an energy transfer time of $1/\gamma_{\text{transfer}} \approx 1.51$ ns. The calculated lifetime of an exciton in the NP−NR superstructure is $1/\gamma^0_{\text{rec}} = 1/(P\cdot\gamma_{\text{rad}} + \gamma^0_{\text{non-rad}} + \gamma_{\text{transfer}}) \approx 1.4$ ns. Regarding the emission intensity, the following emission ratio was calculated: $A \approx 0.07$. Overall, our theoretical data are in qualitative agreement with the experimental data (Table 1 and Figure 2A−B). Importantly, our theory reveals microscopic mechanisms of energy exchange in the NP−NR assemblies. We note that the calculated exciton lifetime in the bioassembly ($1/\gamma_{\text{rec}} \approx 1.6$ ns) is close to the observed lifetime (2 ns) for NP/NR = 125 from Table 1. However, the extrapolated lifetimes for very small NP-NR ratios are essentially shorter (Table 1). We see two possible ways to explain it: (1) extrapolation using the Stern−Volmer kinetics is not always reliable or (2) there may be an additional mechanism of quenching of emission in the system. Considering the trend of

experimental points in Stern−Volmer plot (Figure S1, Supporting Information), which indicates that the for small NP/NW ratios the lifetime becomes shorter, we believe that additional mechanisms of energy transfer/quenching are possible which can be represented by charge transfer reactions.

Finally, the physical reasons why the lifetime strongly depends on the NP/NW ratio should also be discussed. In experiments (Table 1), we clearly see this tendency: the lifetime becomes strongly reduced with decrease of the NP/NR ratio. Physically, this can be explained in the following way: when NP/NR > 70, NPs cannot form a single shell around a NR and arrange themselves in two or more layers. Moreover, even for relatively small NP/NW ratio, not all NPs may form a single shell and be very close to the metal surface. Some of NPs may be on the top of other NPs (see Figure 1). This means that the average NP−NW distance is dependent on NP/NW ratio and therefore, the NP-NW transfer time becomes dependent on it too, becoming shorter when smaller number of NPs is present (Stern−Volmer fit in the Supporting Information, Figure S1).

One can also can notice that the blue shift in Figure 3 is larger for NP/NW = 12.5; this behavior is consistent with the same distance dependence as was described above for lifetimes. For smaller NP/NW ratio (12.5), the blue shift should be indeed larger since NPs are located on average closer to the metal surface and the metal screening effect is stronger. For the larger ratio (125 > 70), the blue shift should be smaller since the average NP−NW distance is increased.

We also should compare the experimental and theoretical emission ratios, A. For the assembled structures with NP/NR = 125, we see a nice overall correspondence of theory and experiment: $A_{\text{theory}} \approx 0.07$ and $A_{\text{exp } er} \approx 0.08$. Finally we should note that the plasmon-induced field enhancement in our system is small, $P_{\text{tot}} \approx 1$. Therefore, the energy transfer process plays the main role and leads to strong emission quenching as opposed to emission enhancement.

Conclusions

We have demonstrated NP−NR superstructures which can act as potential energy transfer pumps and help reduce the absorptive metallic losses. Excitons created optically in NPs become converted into plasmons in metal NRs via the Förster energy transfer mechanism and intermediate exciton-plasmon hybrid resonant state. In this way, the plasmon population inside the metal component can be sustained via off-resonance light adsorption. The excitation wavelength of NPs can be far from the plasmon resonance wavelength of NR, say in UV absorption bands of CdTe, such as 350 nm as we used in this work, hence the emission of NP would interfere minimally with the incident light at optical wavelengths unlike similar systems that can be created from dyes. Additionally, the energy transfer in NP systems is likely to be more efficient than in analogous dye-based structures due to better resonance conditions with plasmons in NRs and fast spin relaxation to match the required one for a particular place on the NRs. We see the need to reveal in greater detail the exciton-plasmon interactions in semiconductor-metal assemblies with Au NRs and potential competing mechanisms of energy relaxation requiring single-particle spectroscopy and pump−probe techniques.

As a part of the concluding remarks, we also want to make two points about applications of such systems for NIMs. (1) The NR from gold or other metal will likely to form the basic structure on the NIM metamaterials. Advanced methods of manufacturing, such as nanoscale lithography,[1−12] self-organization of polymeric block structures, or layer-by-layer deposition, which can also produce layers of NP and NR separated by a thin (1−2 nm) layer of polymer, are probably the most suitable approaches to their manufacturing. Regardless of the method, bioconjugation processes provides a universal method of attaching semiconductor NPs to the base metallic structure. (2) NPs present a natural advantage over the dyes for NIM materials with gain because of much wider absorption spectrum which makes possible separation of pumping light from the spectral window where NIM response can be observed.

Acknowledgment. This work was supported by the National Science Foundation BioSensor Program and AFOSR under MURI Grant No. FA9550-06-1-0337.

Supporting Information Available: Stern−Volmer data. This material is available free of charge via the Internet at http://pubs.acs.org.

References and Notes

(1) Veselago, V. G. Electrodynamics of Substances with Simultaneously Negative Values of Sigma and Mu. *Sov. Phys. Uspekhi-USSR* **1968**, *10* (4), 509.

(2) Pendry, J. B. Negative refraction makes a perfect lens. *Phys. Rev. Lett.* **2000**, *85* (18), 3966–3969.

(3) Pendry, J. B.; Smith, D. R. The quest for the superlens. *Sci. Am.* **2006**, *295* (1), 60–67.

(4) Cory, H.; Shtrom, A. Wave propagation along a rectangular metallic waveguide longitudinally loaded with a metamaterial slab. *Microwave Opt. Tech. Lett.* **2004**, *41* (2), 123–127.

(5) Fang, N.; Zhang, X. Imaging properties of a metamaterial superlens. *Appl. Phys. Lett.* **2003**, *82* (2), 161–163.

(6) Cummer, S. A.; Popa, B. I.; Schurig, D.; Smith, D. R.; Pendry, J., Full-wave simulations of electromagnetic cloaking structures *Phys. Rev. E* **2006**, *74*, (3).

(7) Lezec, H. J.; Dionne, J. A.; Atwater, H. A. Negative refraction at visible frequencies. *Science* **2007**, *316* (5823), 430–432.

(8) Smolyaninov, I. I.; Hung, Y. J.; Davis, C. C. Magnifying superlens in the visible frequency range. *Science* **2007**, *315* (5819), 1699–1701.

(9) Shvets, G. Photonic approach to making a material with a negative index of refraction. *Phys. Rev. B* **2003**, *67* (3), 035109.

(10) Taubner, T.; Korobkin, D.; Urzhumov, Y.; Shvets, G.; Hillenbrand, R. Near-field microscopy through a SiC superlens. *Science* **2006**, *313* (5793), 1595–1595.

(11) Shelby, R. A.; Smith, D. R.; Schultz, S. Experimental verification of a negative index of refraction. *Science* **2001**, *292* (5514), 77–79.

(12) Shalaev, V. M.; Cai, W. S.; Chettiar, U. K.; Yuan, H. K.; Sarychev, A. K.; Drachev, V. P.; Kildishev, A. V. Negative index of refraction in optical metamaterials. *Opt. Lett.* **2005**, *30* (24), 3356–3358.

(13) Zhou, J. F.; Zhang, L.; Tuttle, G.; Koschny, T.; Soukoulis, C. M. Negative index materials using simple short wire pairs. *Phys. Rev. B* **2006**, *73* (4), 041101.

(14) Zhang, S.; Fan, W. J.; Malloy, K. J.; Brueck, S. R. J.; Panoiu, N. C.; Osgood, R. O. Demonstration of metal-dielectric negative-index metamaterials with improved performance at optical frequencies. *J. Opt. Soc. Am. B* **2006**, *23* (3), 434–438.

(15) Dolling, G.; Enkrich, C.; Wegener, M.; Soukoulis, C. M.; Linden, S. Low-loss negative-index metamaterial at telecommunication wavelengths. *Opt. Lett.* **2006**, *31* (12), 1800–1802.

(16) Ponizovskaya, E. V.; Bratkovsky, A. M. Metallic negative index nanostructures at optical frequencies: losses and effect of gain medium. *Appl. Phys. A: Mater. Sci. Process.* **2007**, *87* (2), 161–165.

(17) Podolskiy, V. A.; Alekseyev, L. V.; Narimanov, E. E. Strongly anisotropic media: the THz perspectives of left-handed materials. *J. Mod. Optics* **2005**, *52* (16), 2343–2349.

(18) Ramakrishna, S. A.; Pendry, J. B., Removal of absorption and increase in resolution in a near-field lens via optical gain. *Phys. Rev. B* **2003**, *67*, (20).

(19) Shamonina, E.; Kalinin, V. A.; Ringhofer, K. H.; Solymar, L. Imaging, compression and Poynting vector streamlines for negative permittivity materials. *Electron. Lett.* **2001**, *37* (20), 1243–1244.

(20) Noginov, M. A.; Zhu, G.; Bahoura, M.; Adegoke, J.; Small, C. E.; Ritzo, B. A.; Drachev, V. P.; Shalaev, V. M. Enhancement of surface plasmons in an Ag aggregate by optical gain in a dielectric medium. *Opt. Lett.* **2006**, *31* (20), 3022–3024.

(21) Nikoobakht, B.; El-Sayed, M. A. Preparation and growth mechanism of gold nanorods (NRs) using seed-mediated growth method. *Chem. Mater.* **2003**, *15* (10), 1957–1962.

(22) Gao, J. X.; Bender, C. M.; Murphy, C. J. Dependence of the gold nanorod aspect ratio on the nature of the directing surfactant in aqueous solution. *Langmuir* **2003**, *19* (21), 9065–9070.

(23) Gaponik, N.; Talapin, D. V.; Rogach, A. L.; Hoppe, K.; Shevchenko, E. V.; Kornowski, A.; Eychmuller, A.; Weller, H. Thiol-capping of CdTe nanocrystals: An alternative to organometallic synthetic routes. *J. Phys. Chem. B* **2002**, *106* (29), 7177–7185.

(24) Wang, Y.; Tang, Z. Y.; Tan, S. S.; Kotov, N. A. Biological assembly of nanocircuit prototypes from protein-modified CdTe nanowires. *Nano Lett.* **2005**, *5* (2), 243–248.

(25) Lee, J.; Javed, T.; Skeini, T.; Govorov, A. O.; Bryant, G. W.; Kotov, N. A. Bioconjugated Ag nanoparticles and CdTe nanowires: Metamaterials with field-enhanced light absorption. *Angew. Chem., Int. Ed.* **2006**, *45* (29), 4819–4823.

(26) Gole, A.; Murphy, C. J. Polyelectrolyte-coated gold nanorods: Synthesis, characterization and immobilization. *Chem. Mater.* **2005**, *17* (6), 1325–1330.

(27) Govorov, A. O.; Bryant, G. W.; Zhang, W.; Skeini, T.; Lee, J.; Kotov, N. A.; Slocik, J. M.; Naik, R. R. Exciton-plasmon interaction and hybrid excitons in semiconductor-metal nanoparticle assemblies. *Nano Lett.* **2006**, *6* (5), 984–994.

(28) Lee, J.; Govorov, A. O.; Kotov, N. A. Nanoparticle assemblies with molecular springs: A nanoscale thermometer. *Angew. Chem., Int. Ed.* **2005**, *44* (45), 7439–7442.

(29) Lee, J.; Govorov, A. O.; Kotov, N. A. Bioconjugated superstructures of CdTe nanowires and nanoparticles: Multistep cascade forster resonance energy transfer and energy channeling. *Nano Lett.* **2005**, *5* (10), 2063–2069.

(30) Toyama, T.; Matsune, K.; Oda, H.; Ohta, M.; Okamoto, H. X-ray diffraction study of CdS/CdTe heterostructure for thin-film solar cell: influence of CdS grain size on subsequent growth of (111)-oriented CdTe film. *J. Phys. D* **2006**, *39* (8), 1537–1542.

(31) Govorov, A. O.; Lee, J.; Kotov, N. A. , Theory of plasmon-enhanced Forster energy transfer in optically excited semiconductor and metal nanoparticles. *Phys. Rev. B* **2007**, *76*, (12).

(32) Lee, J.; Dulka, J.; Govorov, A. O.; Kotov, N. A. Bioconjugated cote and Au nanoparticles for energy transport. *Abstr. Pap. Am. Chem. Soc.* **2004**, *228*, U897–U897.

(33) Lee, J.; Govorov, A. O.; Dulka, J.; Kotov, N. A. Bioconjugates of CdTe nanowires and Au nanoparticles: Plasmon-exciton interactions, luminescence enhancement, and collective effects. *Nano Lett.* **2004**, *4* (12), 2323–2330.

(34) Schubert, E. F.; Vredenberg, A. M.; Hunt, N. E. J.; Wong, Y. H.; Becker, P. C.; Poate, J. M.; Jacobson, D. C.; Feldman, L. C.; Zydzik, G. J. Giant Enhancement of Luminescence Intensity in Er-Doped Si/SiO2 Resonant Cavities. *Appl. Phys. Lett.* **1992**, *61* (12), 1381–1383.

(35) Chowdhury, M. H.; Malyn, S. N.; Aslan, K.; Lakowicz, J. R.; Geddes, C. D. Multicolor directional surface plasmon-coupled chemiluminescence. *J. Phys. Chem. B* **2006**, *110* (45), 22644–22651.

(36) Choong, V. E.; Park, Y.; Shivaparan, N.; Tang, C. W.; Gao, Y. Deposition-induced photoluminescence quenching of tris-(8-hydroxyquinoline) aluminum. *Appl. Phys. Lett.* **1997**, *71* (8), 1005–1007.

(37) Lee, J.; Hernandez, P.; Lee, J.; Govorov, A. O.; Kotov, N. A. Exciton-plasmon interactions inmolecular spring assemblies of nanowires and wavelength-based protein detection. *Nat. Mater.* **2007**, *6* (4), 291–295.

(38) Mamedov, A. A.; Belov, A.; Giersig, M.; Mamedova, N. N.; Kotov, N. A. Nanorainbows: Graded semiconductor films from quantum dots. *J. Am. Chem. Soc.* **2001**, *123* (31), 7738–7739.

(39) Wang, S. P.; Mamedova, N.; Kotov, N. A.; Chen, W.; Studer, J. Antigen/antibody immunocomplex from CdTe nanoparticle bioconjugates. *Nano Lett.* **2002**, *2* (8), 817–822.

(40) Landau, L. D.; Lifshitz, E. M. *Quantum mechanics: non-relativistic theory*, 3rd ed.; Pergamon Press: Oxford; New York, 1977; pp xiv, 673.

(41) Persson, B. N. J.; Lang, N. D. Electron-Hole-Pair Quenching of Excited-States near a Metal. *Phys. Rev. B* **1982**, *26* (10), 5409–5415.

(42) Palik, E. D. Handbook of Optical-Constants. *J. Opt. Soc. A* **1984**, *1* (12), 1297–1297.

(43) Rogach, A.; Koktysh, D.; Harrison, M.; Kotov, N. A. *Chem. Mater.* **2000**, *12* (6), 1526–1528.

JP8006238